Physica A 467 (2017) 1–10

Contents lists available at ScienceDirect

Physica A

journal homepage: www.elsevier.com/locate/physa

Digital image communication scheme based on the breakup of spiral waves

Martynas Vaidelys [a], Chen Lu [b,c], Yujie Cheng [b,c], Minvydas Ragulskis [a,*]

[a] Research Group for Mathematical and Numerical Analysis of Dynamical Systems, Kaunas University of Technology, Studentu 50, Kaunas LT-51368, Lithuania

[b] School of Reliability and Systems Engineering, Beihang University, Beijing 100191, China

[c] Science and Technology on Reliability and Environmental Engineering Laboratory, Beijing 100191, China

HIGHLIGHTS

- A digital image communication scheme based on the breakup of spiral waves is developed.
- This communication system does not require spatially homogeneous random initial conditions.
- The secret image is not embedded into the initial conditions of self-organizing patterns.
- Computational experiments are used to demonstrate efficiency of the proposed scheme.

ARTICLE INFO

Article history:
Received 26 July 2016
Available online 5 October 2016

Keywords:
Spiral wave
Self-organizing pattern
Image hiding

ABSTRACT

A digital image communication scheme based on the breakup of spiral waves is presented in this paper. This communication system does not require spatially homogeneous random initial conditions. Moreover, the secret image is not embedded into the initial conditions of the evolving self-organizing patterns. Such features increase the security of the communication, but still enable an effective transmission of the secret image. Computational experiments are used to demonstrate the properties and efficiency of the proposed scheme.

1. Introduction

The science of pattern formation focuses on the mathematical laws governing the formation of such visual images which mimic the evolution of self-organizing patterns in nature. Pattern formation in biology [1–4]. (animal markings, growth of colonies, vegetation patterns, cancer dynamics), chemistry [5–7] (reaction–diffusion systems, Turing patterns), physics [8,9] (liquid crystals, granular material, optical resonators), computer graphics [10,11] (cellular automata, texture analysis) attracts the attention of researches since the middle of the twentieth century.

It is well known that self-organizing patterns can be used for hiding and communicating secret visual images. A digital fingerprint image is employed as the initial condition for the evolution of a pattern using a model of reaction–diffusion cellular automata [12]. A secure steganographic communication algorithm is developed in Refs. [13,14] where patterns are evolved by using a Beddington–DeAngelis type predator–prey model with self- and cross-diffusion. Self-organizing patterns

* Corresponding author.
E-mail addresses: martynas.vaidelys@ktu.lt (M. Vaidelys), luchen@buaa.edu.cn (C. Lu), yujiecheng.ok@163.com (Y. Cheng), minvydas.ragulskis@ktu.lt (M. Ragulskis).

http://dx.doi.org/10.1016/j.physa.2016.09.050
0378-4371/

induced by prisoner-dilemma-type interactions between competing individuals, and described by evolutionary spatial 2×2 games are exploited for hiding and transmitting secret visual information in Ref. [15]. An image communication scheme based on self-organizing patterns produced by the atrial fibrillation model is presented in Ref. [16]. Self-organizing patterns produced by an array of non-diffusively coupled nonlinear maps are exploited to hide digital images in Ref. [17].

Any digital image communication scheme should satisfy several important requirements. First of all, it should be steganographically secure—it should protect not only the concealed secret image, but also the communicating parties [18]. Secondly, it would be advantageous if the communication scheme (especially the decoding of the secret image) is computationally effective. Finally, the communication algorithm must be able to withstand different kind of attacks.

All previously mentioned digital image hiding techniques based on self-organizing patterns do have some sort of deficiencies. The algorithm presented in Ref. [12] is not steganographically secure because the fingerprint image embedded into initial conditions is visible in the evolved pattern. Digital image communication algorithms based on Beddington–DeAngelis type predator–prey model with self- and cross-diffusion [13,14] require huge computational resources—an interpretable pattern starts forming after at least 10 000 time forward steps. The global optimal strategy in evolutionary spatial 2×2 games is not sensitive to local strategy variations of a single payer—large blocks of pixels must be inverted in the matrix of random initial conditions for the technique presented in Ref. [15]. Self-organizing patterns produced by competitively but non-diffusively coupled nonlinear maps [16] are originated by wave propagation in isotropic media, what predetermines a rather low complexity of the pattern structure—and therefore low information capacity of the communication algorithm.

All discussed digital image communication schemes based on self-organizing patterns are based on some sort of modification of initial conditions. The secret image is represented in the form of a dot-skeleton representation and is embedded into a spatially homogeneous random initial state far below the noise level in Refs. [13,14,16,17]. Dichotomous pixels in the initial conditions are inverted in regions corresponding to the secret image in Ref. [15].

As mentioned previously, the self-organization of patterns in all discussed digital image communication schemes [13–17] is induced by spatially homogeneous random initial conditions. The generation of initial conditions is an integral part of all these communication schemes. For example, it is shown in Ref. [16] that a slight variation in the random initial conditions completely compromises the communication algorithm.

In other words, the generation of random initial conditions and an appropriate modification of these initial conditions lies in the backbone of the discussed communication algorithms. Therefore, parameters determining the generation of random initial conditions are the integral part of the set of private and public keys of the communication algorithm. The ability to avoid the necessity of using random initial conditions for the generation of self-organizing pattern would be a serious enhancement in respect of the security of the communication scheme. On the other hand, it would be advantageous if the communication scheme would not use the perturbation of initial conditions. That would prevent the cheating attack to the communication scheme – whereas the eavesdropper would not be able to embed fake secret images – even if all keys of the communication scheme would be compromised (known to the eavesdropper).

The main objective of this paper is to develop such a digital image communication scheme based on self-organizing patterns that would neither use random initial conditions, nor require any perturbations of the initial conditions. Clearly, a new approach is required both to the physical model governing the formation of self-organizing patterns, both to the concept of the communication scheme itself.

This paper is organized as follows. The physical model governing the formation of patterns is presented in Section 2; the formation of the difference image is discussed in Section 3; the proposed communication scheme is presented in Section 4; the communication algorithm is demonstrated in Section 5 and concluding remarks are given in the final section.

2. The spiral wave model

We use the paradigmatic Barkley model [19,20] for modeling spiral waves in excitable and oscillatory media. The considered model comprises a system of reaction–diffusion equations describing the interaction of the activator u and the inhibitor v:

$$\frac{\delta u}{\delta t} = f(u, v) + \nabla^2 u, \qquad \frac{\delta v}{\delta t} = g(u, v) + D\nabla^2 v \tag{1}$$

where $f(u, v)$ and $g(u, v)$ are local reaction kinetics functions and the parameter D is then the ratio of diffusion coefficients. The reaction term $f(u, v)$ is given by:

$$f(u, v) = \frac{h(x)}{\epsilon} u(1 - u)(u - u_{th}(v)) \tag{2}$$

where the parameter ϵ sets the timescale separation between the fast u-equation and the slow v-equation (therefore ϵ is typically small); functions $h(x)$ and $u_{th}(v)$ define the evolution of the slow variable. In the simplest case [19]:

$$h(x) = 1, \qquad u_{th}(v) = \frac{v - b}{a} \tag{3}$$

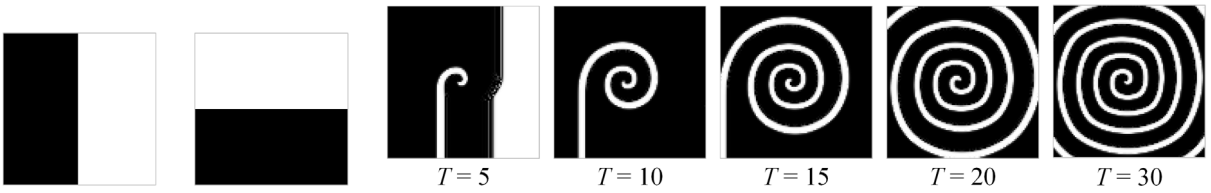

(a) Initial u-field. (b) Initial v-field. (c) Pattern, u-field.

Fig. 1. The evolution of a regular spiral wave. The parameters of the model are set to: $L = 100, \epsilon = 0.02, a = 0.75, b = 0.02, g = u - v$; d$t = 0.05$. Initial conditions are shown in parts a and b; the evolution of the u-field—in part c.

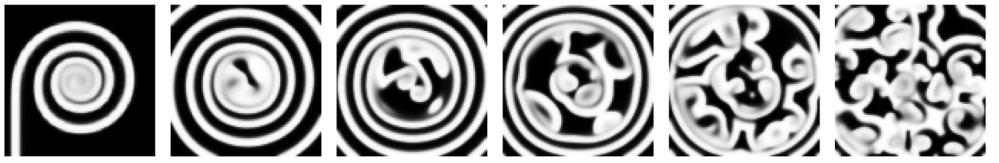

Fig. 2. The evolution of a spiral wave with breakups (u-field only) with parameters set to: $\epsilon = 0.075, b = 0.0006, g = u^3 - v$ (other parameters are the same as in Fig. 1).

where a and b are system parameters—larger a gives a longer excitation duration and higher ratio b/a gives a larger excitability threshold. The other reaction term reads:

$$g(u, v) = u - v. \tag{4}$$

The nullclines in the Barkley model for the nonlinear u reaction kinetics are straight lines. The u-nullclines are given by $f(u, v) = 0$ so that the three branches are:

$$u = \begin{cases} 0, \\ u_{th}(v), \\ 1. \end{cases} \tag{5}$$

The middle branch sets the excitation threshold. In practice, for spiral wave solutions, the system does not pass through the corners where branches of the nullclines intersect.

This reaction is simulated with a simple Euler forward scheme; the Laplacian is simulated numerically using a finite differences method on a regular square grid with a five-point formula [20]:

$$\frac{\nabla^2 u}{4} = \frac{1}{4}\left(u_{i+1,j} + u_{i-1,j} + u_{i,j+1} + u_{i,j-1}\right) - u_{i,j}. \tag{6}$$

Combining five-point formula with large time steps the reaction terms can be time stepped with relatively little computational efforts.

The domain is represented as a 2D square of size L with zero-flux boundary conditions. We set the initial conditions as dichotomous patches (vertical for the u-field and horizontal for the v-field) where the black color corresponds to 0 and the white color—to 1 (Fig. 1). In such a model the spiral wave is forming with no sign of breakup [19]. The time step dt is set to 0.05; the time period used for the computation is marked as T. The evolving spiral wave is illustrated at $T = 5$, 10, 15, 20 and 30 in Fig. 1.

A regular spiral wave may evolve into a non-regular spiral wave with breakups when the reaction term g is a nonlinear function (as suggested in Ref. [21]):

$$g(u, v) = u^3 - v. \tag{7}$$

As discussed in Ref. [22], there are sets of parameters a, b and ϵ the spirals may undergo period rotations or various types of meander/break-ups. The evolution of the pattern into a complete breakage is illustrated in Fig. 2.

3. The formation of the difference image

The construction of a digital image communication scheme based on self-organizing patterns requires the formation of two patterns. The nonlinear model of the system governs the evolution of one pattern from a predetermined set of initial conditions—while the evolution of the second one is started from the perturbed initial conditions [13–17]. The secret image leaks in a form of a difference image between these two patterns. The morphological operation describing the difference pattern reads:

$$D(i, j) = abs\left(P(i, j) - \tilde{P}(i, j)\right) \tag{8}$$

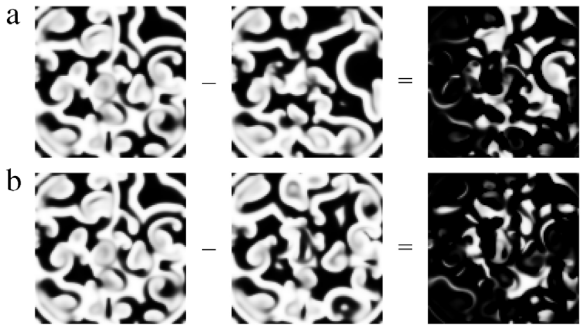

Fig. 3. The formation of patterns is sensitive to a perturbation of even 1 pixel in the initial conditions. Part (a) shows the pattern which forms from the initial u-field when the whole right part of the u-field is perturbed from 1 to 0.99. Part (b) shows the pattern which forms when a single pixel of the u-field is inverted. Remarkably, the complexity of the resulting difference images is not much different.

where $P(i,j)$ and $\tilde{P}(i,j)$ are the grayscale levels of the pixel (i,j) in the first and the second patterns; $D(i,j)$ denotes the difference pattern. Thus, the difference image is black if two patterns are identical.

We will use several different perturbations in the initial conditions to illustrate the formation of difference images in the model of the spiral wave with breakups. The parameters of the system are kept the same as described in Fig. 2; the time interval used for the evolution of the pattern is set to $T = 70$. The initial values of the v-field are kept the same as in Fig. 2; the initial values of the u-field are modified by changing the numerical value in the right part of the field from 1 to 0.99. Such perturbation of initial conditions is similar to the perturbation used in Ref. [15] where an inversion of a single pixel does not change the self-organizing pattern and the manipulation with blocks of pixels is required for generating any changes in the difference image.

The left image in row (a) in Fig. 3 shows the unmodified pattern P (this is the same image as the rightmost pattern in Fig. 2). The middle image in row (a) in Fig. 3 is the pattern $\tilde{P}$ evolved from the modified initial conditions. The right image in row (a) in Fig. 3 is the difference pattern between P and $\tilde{P}$. It can be seen that the perturbation in the initial conditions has spread in the whole domain. Moreover, this perturbation is clearly visible in the difference image—no contrast enhancement techniques are required to visualize the pattern in the difference image. This is a serious improvement compared to previously proposed digital image communication schemes where contrast enhancement of the difference image is an integral part of these schemes [13–17].

However, it appears that the evolution of spiral waves to breakups is sensitive to perturbations even at one single pixel of the initial conditions. The middle image in row (b) in Fig. 3 shows the pattern that evolved from the initial values identical to ones used in Fig. 2 except one pixel at the center of the image—its value is perturbed from 1 to 0.99. Remarkably, the complexity of the difference image is comparable to the one in the previous computational experiment (Fig. 3 row (a)).

It is clear that a simple perturbation of initial conditions would not be applicable for the construction of the digital image communication scheme based on the breakup of spiral waves—a slight perturbation of a single pixel results into the alternation of the complete pattern. That can be explained by a long time required for the evolution of the pattern and the unpredictable avalanche-type formation of the breakups. However, shorter time intervals cannot be used either—the pattern is simply undeveloped then (Fig. 2). Another type of algorithm should be designed in order to replicate the communication scheme presented in Refs. [13–17].

4. The proposed scheme

As mentioned previously, a perturbation of initial conditions cannot be exploited for hiding a secret image in the self-organizing pattern produced by the breakup of spiral waves. And while the evolution of the first pattern from random initial conditions is not altered, the evolution of the second pattern should be perturbed in a different way (if compared to Refs. [13–17]). A possible solution is to perturb the second pattern not at the beginning of its evolution—but at some moment before the evolution of both patterns is terminated.

4.1. Delayed perturbation at a discrete point

Let us repeat the computation experiment presented in Fig. 3—except that the perturbation into the second pattern is introduced at time moment $T = 57.5$ and the evolution of both patterns is terminated at $T = 60$ (initial conditions are the same as earlier; $L = 50$; $\epsilon = 0.1$; $a = 0.7$; $b = 0.06$; $g = u^3 - v$; $\mathrm{d}t = 0.05$). We do perturb one pixel at the center of the second pattern by adding 5% to its value at $T = 57.5$ (Fig. 4). The unperturbed pattern at $T = 57.5$ is shown in Fig. 4(a); the perturbed image—in Fig. 4(b) (the perturbation is so small that it is invisible to a naked eye). The perturbation point is clearly visible in the difference image at $T = 57.5$ in Fig. 4(c)—the grayscale range is automatically adjusted to max–min levels in the image.

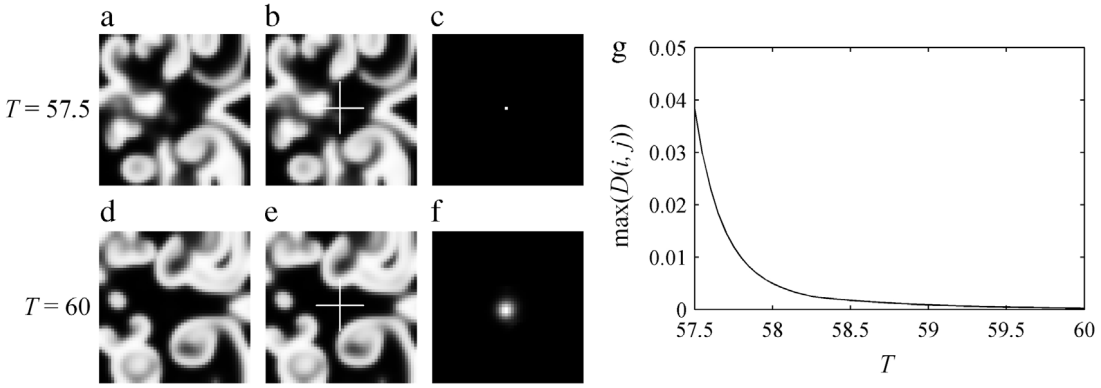

Fig. 4. Perturbation is introduced at time $T = 57.5$ by adding +5% to the u-field at the center point of the image. Part (a) shows the unperturbed pattern at $T = 57.5$; (b)—the perturbed pattern at $T = 57.5$ (the white cross denotes the perturbed pixel); (c)—the difference image between the perturbed and the unperturbed patterns at $T = 57.5$. The unperturbed, the perturbed pattern and the difference image at $T = 60$ are shown in parts (d), (e) and (f). The decay of the maximum value of the u-field in the difference image over time is illustrated in part (g).

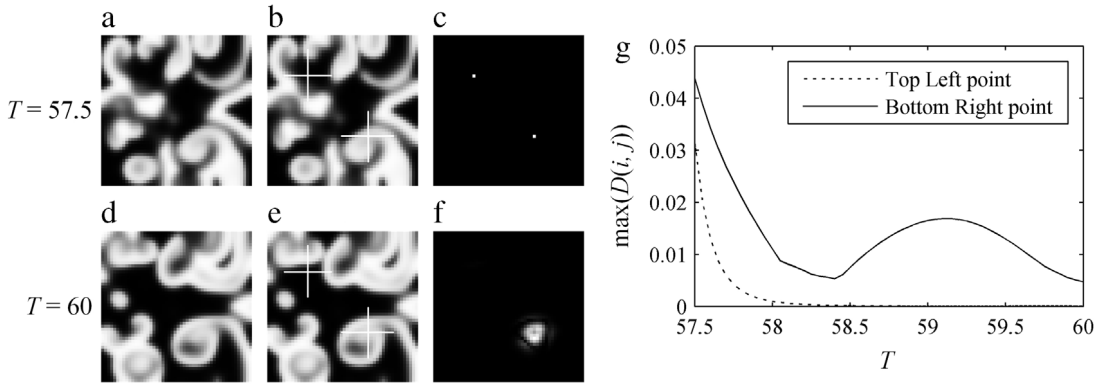

Fig. 5. The perturbation at the top left point is introduced in the area where no new breakup waves occur during the rest of simulation; thus the maximum intensity of the spot in the difference image decreases monotonically. However, the bottom right perturbation point is located in the area where multiple breakup waves pass until the simulation is terminated. That results in the fluctuation of intensity of the spot in the difference image.

The maximum value of the u-field in the difference image in Fig. 4(c) is 0.0372 and is illustrated in Fig. 4(g) at $T = 57.5$. Fig. 4(d) shows the unperturbed pattern; Fig. 4(e)—the perturbed pattern at $T = 60$. The initial perturbation at one pixel (Fig. 4(c)) diffuses as the patterns continue to evolve (Fig. 4(f)). However, the maximum value of the u-field in the difference image quickly decreases as the time goes on (Fig. 4(g)). The only reason why the diffused region is well visible in Fig. 4(f) is due to the automatic adjustment to max–min levels (the same procedure as used in Fig. 4(c)).

However, it appears that the decay of the contrast of the perturbed pixel is not always monotonic and depends on the location of the pixel in respect to the breaking waves (Fig. 5). Two pixels are perturbed at $T = 57.5$ (Fig. 5(b)). However, the evolution of the perturbations in the difference image is completely different (Fig. 5(g)). This effect can be explained by the interaction between the perturbation and the propagating front of the breaking spiral wave. The top left point remains in the calm zone during the whole time interval of evolution $57.5 \ll T \ll 60$ (Fig. 5(b); (e)). On the contrary, the bottom right point is located in the region of the formation of the breakup wave. It appears that the interaction of the perturbation with the propagating wave front causes a temporary amplification of the perturbation effect and a complex pattern formation in the difference image around the perturbation point (Fig. 5(f)). Moreover, the effects caused by the perturbation at the top left point are completely overwhelmed by the effects caused by the perturbation at the bottom right point (Fig. 5(f)). Therefore, the evolution of the pattern in the difference image is sensitive to the geometrical location of the perturbation point in respect to the evolving front of the propagating breakup wave. It is clear that a strategy based on straightforward perturbations of the evolving pattern at a preselected set of points would not be applicable for hiding a secret in the difference image.

4.2. The equalization of maximum intensities in the difference image

A possible solution to the problem associated to different decay rates of the perturbation intensities at different locations of the evolving pattern could be based on the variation of time moments of perturbations at different points. Such

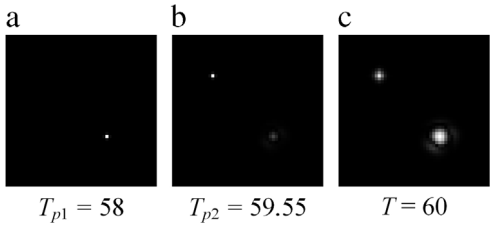

Fig. 6. The equalization of maximum intensities of perturbations in the difference image. The perturbation at the bottom right point (p_1) is performed at $T = 58$ (part a); the perturbation at the top left point (p_2) is performed at $T = 59.55$ (part b). The perturbations evolve differently due to different interaction with the propagating front of the breakup waves (part c).

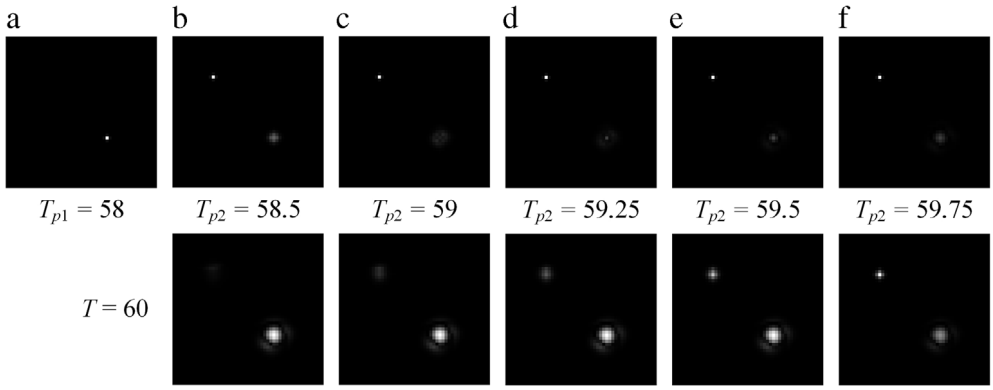

Fig. 7. The comparison of difference images when the bottom point (p_1) perturbation is fixed at time $T = 58$ and the top point (p_2) perturbation time varies. Corresponding difference image (at $T = 60$) is provided in the second row of images.

equalization of maximum intensities at the difference image in Fig. 5(f) is illustrated in Fig. 6. We repeat the computational experiment, but only the bottom right point is perturbed at $T = 58$ (the difference image is shown in Fig. 6(a)). The intensity of the perturbation at the bottom right point starts to decay—and we perturb the top left point at $T = 59.55$ (Fig. 6(b)). The perturbation at the bottom right point starts interacting with the propagating front of the breakup wave—and the intensity of the difference image around this point starts increasing; the maximum intensities of perturbations around two points in the difference image become equal at $T = 60$ (Fig. 6(c)).

It is clear that the selection of proper time moments of the perturbation is a complex problem—everything depends on the location of the perturbation points and the particular dynamical distribution of the evolving pattern of breakup waves. The complexity of the problem is illustrated in Fig. 7. All parameters of the system (including the geometrical locations of the two perturbation points) are kept the same. The only varying parameter is the time moment of the perturbation at the top left point (denoted as T_{p2} in Fig. 7). The bottom right point (p_1) is perturbed at $T = 58$ (Fig. 7(a)). Then, five independent computational experiments are executed by perturbing the pattern at the top left point (p_2) at $T = 58.5$ (Fig. 7(b)); $T = 59$ (Fig. 7(c)); $T = 59.25$ (Fig. 7(d)); $T = 59.5$ (Fig. 7(e)) and $T = 59.75$ (Fig. 7(f)). Figures at the top row show the difference image at the moment of perturbation; figures at the bottom row—the difference image at $T = 60$. As mentioned previously, the evolution of a perturbation depends on the interaction with the propagating front of the breakup wave. Anyway, it is possible to find such T_{p2} where the maximum intensities of evolved perturbations in the difference image at $T = 60$ are almost the same (Fig. 7(e))—though the "deformations" around points p_1 and p_2 are different.

4.3. The equalization of both intensities and shapes

Such manipulation with time moments of the perturbation at different points of the evolving pattern can yield the same maximum intensity at both points in the difference image. However, the size of the deformations around the perturbed points (in the difference image) is clearly different (Fig. 6(c)). It would be almost impossible to use such a perturbation strategy for a meaningful hiding of the secret image. A new perturbation strategy should be used in order to overcome this limitation.

We continue the same computational experiment as described in Fig. 6—however we change the perturbation around point p_2. Instead of perturbing the evolving pattern at a single point, we perturb 6 adjacent points around p_2 (Fig. 8(b)). Note that the intensity of perturbations is kept the same at all 6 points; the specific geometrical location of the perturbed points is adjusted experimentally in order to produce such a difference image that both intensities and geometric shapes of the deformations are almost identical in the difference image (Fig. 8(c)).

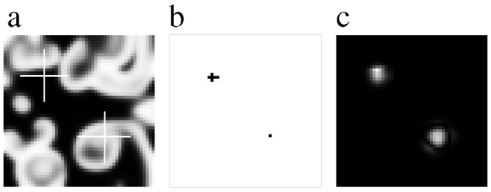

Fig. 8. The adaptive perturbation strategy helps to equalize both the intensities and shapes of spots in the difference image. The location of the perturbation points is the same as in Fig. 5. The perturbation at the bottom right point (p_1) is performed at $T = 57.8$; the perturbation at the top left point (p_2) is performed at $T = 56$. Six points around the point p_2 are perturbed; the intensity of the perturbation at all points is the same as before.

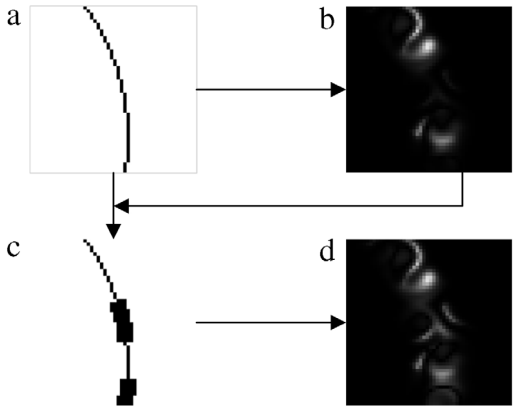

Fig. 9. The illustration of the iterative process of the formation of the perturbation. A thin line type perturbation (part (a)) yields the difference image with an undeveloped inner part (part (b)). The perturbation is strengthened in those parts where the difference image is not clear enough (part (c)) and the computational experiment is repeated again till the difference image is clear enough (part (d)).

4.4. The formation of geometric primitives in the difference image

The ability to control the shape and the intensity of the deformations in the difference image allows a possibility to construct different shapes and geometrical primitives. We continue the computational experiments with the same set of parameters—except that the dimensions of the area used for the pattern formation are now 500 × 500 pixels (Fig. 9). The intensity of perturbations is kept the same by adding +5% to the u-field—but instead of perturbing a single point we do perturb all points on the circle (Fig. 9(a)). The perturbation is performed at $T = 145$; the system continues to evolve until $T = 150$. The final pattern produced after the perturbation is shown in Fig. 9(b); the difference image—in Fig. 9(c).

It is natural to expect that the produced ring in the difference image is discontinuous—the formation of the difference image is sensitive to the geometrical locations of the propagating fronts of the breakup waves. One of the possibilities to make the geometric object more comprehensible in the difference image is to increase the area of perturbation (Fig. 9(d)). However, though the discontinuities become smaller, the differences between the highest and the lowest intensities in the difference image are still large (Fig. 9(f)).

4.5. Adaptive perturbation strategy

A strategy for the equalization of intensities and shapes is also required for geometric primitives in the difference image. A possible adaptive solution to the problem is schematically illustrated in Fig. 9. Let us assume that the perturbation (Fig. 9(a)) results into the difference image as shown in Fig. 9(b). The discontinuities in the difference image can be detected by using manual, semi-automatic or even completely automatic means. Then, the perturbation must be adaptively tuned in order to eliminate the discontinuities (Fig. 9(c)). In general, the variation of the perturbation is sensitive to almost all parameters of the system—including the moment of the perturbation and the final time moment when the evolution of patterns is terminated. In our computational setup it is enough to enlarge the width of the perturbation line from a one-pixel line to a 5-pixels line (Fig. 9(c)). That is sufficient to ensure that the discontinuities in the difference image disappear (Fig. 9(d)).

The same adaptive strategy is now applied to the computational experiment presented in Fig. 10. The discontinuities and zones of lower intensity are detected in Fig. 10(c); the perturbation is adaptively corrected (Fig. 10(d)). The resulting difference image now clearly represents a regular geometric shape (Fig. 10(f)).

Note that the presented adaptive strategy of the perturbation does not exploit the variation of time delays used to perform the perturbation at different locations of the digital image. Application of such features could enhance the difference image even more—but we limit the functionality of the proposed communication algorithm by excluding these time-related aspects.

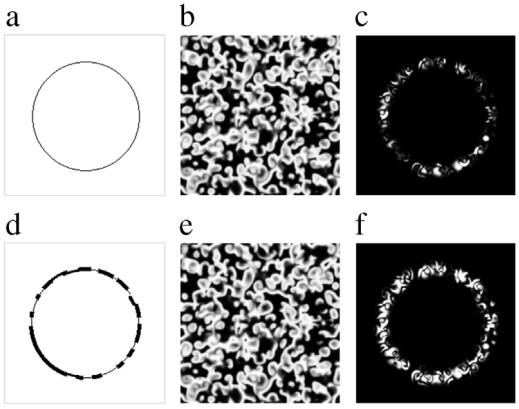

Fig. 10. The adaptive perturbation strategy for the formation or a ring in the difference image. A thin circle-type perturbation (part (a)) is applied to the pattern at $T = 145$. The resulting pattern at $T = 150$ is shown in part (b); the difference image (at $T = 150$)—in part (c). The adaptive perturbation strategy is used to modify the perturbation (part (d)). The resulting pattern (at $T = 150$) is shown in part (e); the difference image—in part (f). The set of system parameters is: $\epsilon = 0.1$; $a = 0.7$; $b = 0.06$.

5. The communication algorithm

The proposed communication algorithm based on the breakup of spiral waves is illustrated by the following diagram (Fig. 11). Let us consider two communication parties—Bob and Alice. Bob transmits a secret digital image to Alice. The action steps to be taken by Bob are bordered by a thick dashed line; the steps to be taken by Alice are enclosed into a gray-shaded area (Fig. 11).

5.1. Encoding of the secret image

Initially (at $T = 0$), Bob selects initial conditions of the u-field and the v-field as shown in Fig. 11. Note that generation of random initial conditions is not required for this communication scheme—what is a serious advantage compared to other communication algorithms based on the self-organizing patterns.

Then, Bob stops the evolution of the spiral waves at $T = 145$ and perturbs it at the points corresponding to the secret image (by adding 5% to appropriate pixels of the u-field). Bob continues to evolve the perturbed pattern until $T = 150$ (100 time forward steps from the moment of perturbation). At the same time, Bob evolves the pattern from the initial conditions without any perturbations until the final time moment $T = 150$. That allows Bob to check how the difference image between the perturbed and unperturbed patterns looks like (Fig. 11).

Now, Bob uses the adaptive perturbation strategy and repeats the computational simulation of the perturbed and unperturbed patterns. Proper adjustment of the perturbation points ensures that the difference image is sufficiently clear and representative (Fig. 11). Then, Bob transmits the perturbed pattern to Alice. Note that the perturbation is performed at $T = 145$ and the transmitted pattern is fixed at $T = 150$. Moreover, 100 forward time steps do completely hide the perturbation in the pattern of the spiral waves. No algorithms (statistical or deterministic) could detect any perturbation in this pattern. Also (even all system parameters would be known to the eavesdropper), time backward evolution of the model is impossible due to the nonlinearity of the governing evolutionary equations. The secret digital information is securely embedded into the pattern of spiral waves.

5.2. Decoding the secret image

The decoding process is straightforward. Alice uses the identical initial conditions and evolves the pattern until $T = 150$. Then, she simply computes the difference image between the evolved and the received patterns—the resulting image reveals the secret (Fig. 11).

5.3. Sensitivity of the communication scheme to the perturbation of parameters

The presented decoding process does function only when all system parameters are preset and available both to the Sender and the Receiver. Slight changes of these parameters (when Bob and Alice use different parameters) may compromise the communication scheme.

The sensitivity of the communication scheme to initial parameters is presented in Fig. 12; all illustrations represent difference images only. Initially, we perturb the pattern evolution time by a single integration step. Bob creates the pattern using the previously set parameters ($T = 150$; $\epsilon = 0.1$; $a = 0.7$; $b = 0.06$). However, Alice stops the evolution of her

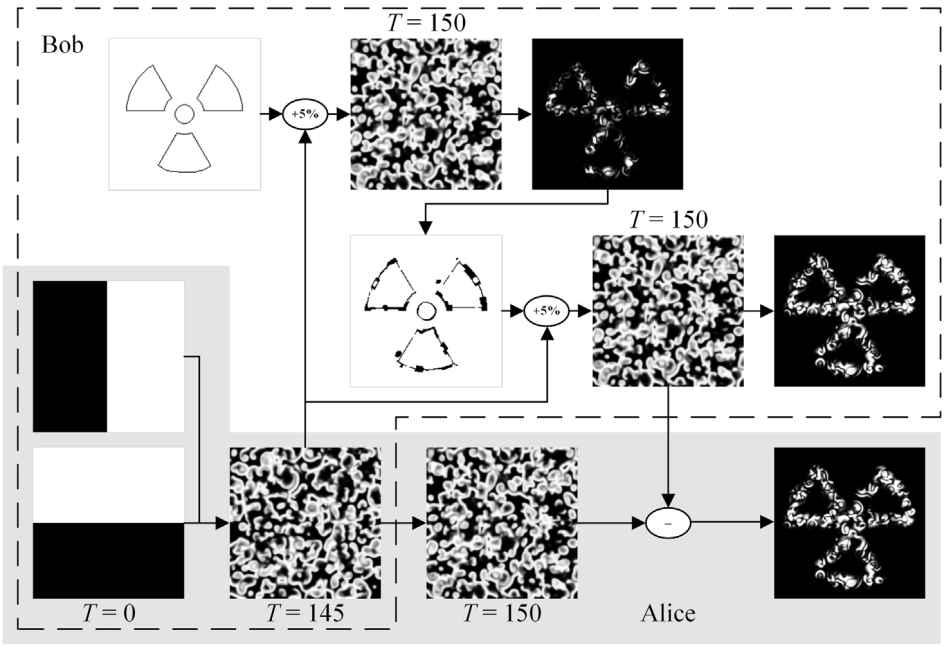

Fig. 11. The schematic diagram of the digital image communication scheme based on the breakup of spiral waves.

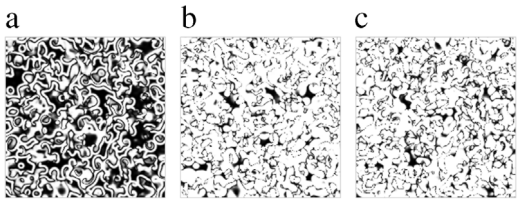

Fig. 12. Slight perturbations of the system parameters compromise the communication system. The set of parameters used by Bob is: $T = 150$; $\epsilon = 0.1$; $a = 0.7$; $b = 0.06$. A slight perturbation of any of these parameters by Alice results into an uninterpretable difference image (a separate perturbation of a single parameter is used in every part respectively): (a) $T = 149.95$; (b) $a = 0.69$; (c) $b = 0.061$.

pattern evolution at $T = 149.95$ instead of $T = 150$. Spiral waves evolve in every iteration—thus Bob's and Alice's patterns are different enough to become useless (Fig. 12(a)).

The next computational experiment simulates the changes of the parameters a and b. Alice mistreats the parameter a by using $a = 0.69$ instead of $a = 0.7$. The change is crucial enough to make the difference image (Fig. 12(b)) uninterpretable. Analogously, the parameter $b = 0.061$ is used instead of $b = 0.06$. The resulting difference (Fig. 12(c)) is meaningless.

5.4. Concluding remarks

A digital image communication scheme based on breaking spiral waves is presented in this paper. The proposed communication scheme does not use random initial conditions for the pattern formation and does not use any perturbations of the initial conditions in order to conceal and transmit the secret digital image. Such computational setup does have a number of serious advantages compared to all communication systems based on self-organizing patterns which had been introduced so far. The sender and the receiver of the image does not require to worry about keeping any keys (private or public) which would determine the generation of initial random conditions. Moreover, the communication algorithm does not use any perturbations of the initial conditions (any dot-skeleton representations or inversions of the dichotomous pixels). Such an approach could be considered as a serious step forward in respect of the security of the communication algorithm.

The evolving pattern is perturbed – not at the beginning – but in the middle of the pattern formation process. It appears that this perturbation is sensitive to the geometrical locations of the traveling fronts of the breakup waves. Therefore, a special adaptive perturbation technique is required for a proper embedding of the secret image into the evolving pattern. However, this adaptive perturbation procedure does not impact the decoding of the secret image. The decoding process remains simple and straightforward—the receiver of the secret image needs just to reproduce the unperturbed pattern of breakup waves.

So far, we had employed the adaptiveness of the perturbation only in the sense of the area of the perturbation in the zones where the difference image appears to be not clear enough. However, the perturbation could be adapted not only in space but also in time (as demonstrated in Fig. 8). The development of a fully automatic adaptive perturbation technique in space and in time remains a definite objective for the future research.

Acknowledgment

Financial support from the Lithuanian Science Council under Project No. MIP-078/2015 is acknowledged.

References

[1] H. Meinhardt, Models of Biological Pattern Formation, Academic Press, 1982.
[2] G.H. Lionel, Kinetic Theory of Living Pattern, Cambridge University Press, 1993, http://dx.doi.org/10.1017/CBO9780511529726.
[3] W. Wang, Y. Lin, L. Zhang, F. Rao, Y. Tan, Complex patterns in a predatorprey model with self and cross-diffusion, Commun. Nonlinear Sci. Numer. Simul. 16 (4) (2011) 2006–2015. http://dx.doi.org/10.1016/j.cnsns.2010.08.035, URL http://www.sciencedirect.com/science/article/pii/S1007570410004697.
[4] Q. Zheng, J. Shen, Dynamics and pattern formation in a cancer network with diffusion, Commun. Nonlinear Sci. Numer. Simul. 27 (13) (2015) 93–109. http://dx.doi.org/10.1016/j.cnsns.2015.02.023, URL http://www.sciencedirect.com/science/article/pii/S1007570415000702.
[5] D. Zhang, L. Gyorgyi, W.R. Peltier, Deterministic chaos in the belousov-zhabotinsky reaction: Experiments and simulations, Chaos 3 (4) (1993) 723–745. http://dx.doi.org/10.1063/1.165933.
[6] P. Grindrod, The Theory and Applications of Reaction–diffusion Equations: Patterns and Waves, in: Oxford Applied Mathematics and Computing Science Series, Clarendon Press, 1996, URL https://books.google.lt/books?id=B9F8QgAACAAJ.
[7] A.M. Turing, The chemical basis of morphogenesis, Philos. Trans. R. Soc. Lond. B Biol. Sci. 237 (641) (1952) 37–72. http://dx.doi.org/10.1098/rstb.1952.0012, arXiv:http://rstb.royalsocietypublishing.org/content/237/641/37.full.pdf, URL http://rstb.royalsocietypublishing.org/content/237/641/37.
[8] J.P. Gollub, J.S. Langer, Pattern formation in nonequilibrium physics, Rev. Modern Phys. 71 (1999) 396–403. http://dx.doi.org/10.1103/RevModPhys.71.S396, URL http://link.aps.org/doi/10.1103/RevModPhys.71.S396.
[9] C.O. Weiss, Y. Larionova, Pattern formation in optical resonators, Rep. Progr. Phys. 70 (2) (2007) 255. URL http://stacks.iop.org/0034-4885/70/i=2/a=R03.
[10] E. Bilotta, P. Pantano, F. Stranges, Computer graphics meets chaos and hyperchaos. some key problems, Comput. Graph. 30 (3) (2006) 359–367. http://dx.doi.org/10.1016/j.cag.2006.02.003, URL http://www.sciencedirect.com/science/article/pii/S0097849306000586.
[11] U. Sahin, S. Uguz, H. Akn, I. Siap, Three-state von neumann cellular automata and pattern generation, Appl. Math. Model. 39 (7) (2015) 2003–2024. http://dx.doi.org/10.1016/j.apm.2014.10.025, URL http://www.sciencedirect.com/science/article/pii/S0307904X14004983.
[12] Y. Suzuki, T. Takayama, I.N. Motoike, T. Asai, Striped and spotted pattern generation on reaction–diffusion cellular automata - theory and LSI implementation, Int. J. Unconv. Comput. 3 (1) (2007) 1–13. URL http://www.oldcitypublishing.com/IJUC/IJUCabstracts/IJUC3.1abstracts/IJUCv3n1p1-13Suzuki.html.
[13] L. Saunoriene, M. Ragulskis, Secure steganographic communication algorithm based on self-organizing patterns, Phys. Rev. E 84 (2011) 056213. http://dx.doi.org/10.1103/PhysRevE.84.056213, URL http://link.aps.org/doi/10.1103/PhysRevE.84.056213.
[14] K. Ishimura, K. Komuro, A. Schmid, T. Asai, M. Motomura, Image steganography based on reaction diffusion models toward hardware implementation, Nonlinear Theory Appl. IEICE 5 (4) (2014) 456–465. http://dx.doi.org/10.1587/nolta.5.456.
[15] P. Ziaukas, T. Ragulskis, M. Ragulskis, Communication scheme based on evolutionary spatial games, Physica A 403 (2014) 177–188. http://dx.doi.org/10.1016/j.physa.2014.02.027, URL http://www.sciencedirect.com/science/article/pii/S0378437114001290.
[16] M. Vaidelys, J. Ragulskiene, P. Ziaukas, M. Ragulskis, Image hiding scheme based on the atrial fibrillation model, Appl. Sci. 5 (4) (2015) 1980. http://dx.doi.org/10.3390/app5041980, URL http://www.mdpi.com/2076-3417/5/4/1980.
[17] M. Vaidelys, P. Ziaukas, M. Ragulskis, Competitively coupled maps for hiding secret visual information, Physica A 443 (2016) 91–97. http://dx.doi.org/10.1016/j.physa.2015.09.044, URL http://www.sciencedirect.com/science/article/pii/S0378437115007803.
[18] S. Katzenbeisser, F.A. Petitcolas (Eds.), Information Hiding Techniques for Steganography and Digital Watermarking, first ed., Artech House, Inc., Norwood, MA, USA, 2000.
[19] D. Barkley, M. Kness, L.S. Tuckerman, Spiral-wave dynamics in a simple model of excitable media: The transition from simple to compound rotation, Phys. Rev. A 42 (1990) 2489–2492. http://dx.doi.org/10.1103/PhysRevA.42.2489, URL http://link.aps.org/doi/10.1103/PhysRevA.42.2489.
[20] M. Dowle, R.M. Mantel, D. Barkley, Fast simulations of waves in three-dimensional excitable media, Int. J. Bifurcation Chaos 7 (1997) 2529–2546.
[21] M. Bär, M. Eiswirth, Turbulence due to spiral breakup in a continuous excitable medium, Phys. Rev. E 48 (1993) 1635–1637. http://dx.doi.org/10.1103/PhysRevE.48.R1635, URL http://link.aps.org/doi/10.1103/PhysRevE.48.R1635.
[22] D. Barkley, Barkley model, Scholarpedia 3 (11) (2008) 1877. http://dx.doi.org/10.4249/scholarpedia.1877, URL http://www.scholarpedia.org/article/Barkley_model.